



Fano Resonance Based on Coupling Between Nanoring Resonator and MIM Waveguide for Refractive Index Sensor

Zain Elabdeen A. Mohamed¹ · Sofyan A. Taya² · Abdulkarem H. M. Almawgani³ · Ayman Taher Hindi³

Received: 20 July 2023 / Accepted: 16 August 2023

© The Author(s), under exclusive licence to Springer Science+Business Media, LLC, part of Springer Nature 2023

Abstract

Fano resonance is a sharp and asymmetric spectral feature that can be used for refractive index sensing. In this paper, we propose a Fano resonance sensor based on the coupling between a nanoring resonator and a metal-insulator-metal (MIM) waveguide. The nanoring resonator is fabricated in the middle of the MIM waveguide, and the two structures are coupled with high-field confinement. The transmission spectrum of the coupled structure shows a Fano resonance, which is sensitive to the refractive index of the surrounding medium. The sensitivity of the sensor is estimated to be 1700 nm/RIU, which is comparable to the sensitivities of other Fano resonance sensors. In addition, the designed sensor achieves the first-ever FOM and Q factor values of 4300.25 RIU⁻¹ and 4310, respectively, for plasmonic MIM sensors. The proposed sensor is simple to fabricate and can be used for a wide range of refractive index sensing applications.

Keywords Plasmonic sensors · Nanoring resonators · Refractive index · Optical sensors

Introduction

Plasmonic sensors are a type of sensor that uses the surface plasmon resonance (SPR) effect to detect the presence of analytes. SPR is a phenomenon that occurs when light interacts with a dielectric metal surface and provides high-field confinement at a sub-wavelength scale. Recently, the metal-insulator-metal (MIM) waveguides based on SPR attract high attention for designing highly integrated optical sensors [1, 2]. Such plasmonic waveguides with simple fabrications and high-field localization represented the most promising candidate in several applications. MIM waveguides are designed and demonstrated for amplifiers [3, 4], detectors [5, 6], plasmonic filters [7–10], switches [11–13], and plasmonic sensors [14–16]. However, such building structures can be demonstrated using photonic crystal structures and plasmonic structures, providing less area

and easy fabrication when compared with photonic crystals. In the last few years, optical plasmonic sensors technology has been fast developed for refractive index (RI) sensing due to good-sensing performance and high-field localization. The sensing mechanism of plasmonic sensors is due to the interaction of incident light on the metal surface that excited the sensing element and generates a highly localized field that is very sensitive to any change in the surrounding RI around the metal [5]. Despite the challenges, plasmonic sensors using silver and air nanosensors are promising new technology with a wide range of potential applications. The silver generates a strong electromagnetic field that can interact with the analyte molecules. The air gaps between the metals provide a region of low RI which can further enhance the sensitivity of the sensor. Consequently, plasmonic sensors using silver and air have been used to detect a wide variety of analytes, including DNA, proteins, and viruses. They have also been used to detect chemicals, pollutants, and toxins [17–21]. To design a high-performance plasmonic sensor, two significant parameters should take into consideration sensitivity and figure of merit (FOM). Sensitivity is directly proportional to the ability of the sensor to detect RI change while FOM provides information about optical signal and is inversely proportional to the bandwidth of resonance dip or peak [22]. Many plasmonic optical sensors are verified in the last few years with various nanostructures for RI

✉ Zain Elabdeen A. Mohamed
zain0011@aun.edu.eg

¹ Physics Department, Faculty of Science, Assiut University, Assiut 71516, Egypt

² Physics Department, Islamic University of Gaza, P.O. Box 108, Gaza, Palestine

³ Electrical Engineering Department, College of Engineering, Najran University, Najran, Kingdom of Saudi Arabia

sensing in the infrared region of the spectrum. Khani et al. [23] designed a plasmonic RI sensor based on plasmon-induced transparency with maximum sensitivity and FOM of 725.1 nm/RIU and 91.78 RIU⁻¹, respectively. Fang et al. [24] investigated the sensing performance of a semi-ring rectangular composite cavity with sensitivity and FOM value of 1260.5 nm/RIU and 41.67 dB, respectively. Other previously reported structures, such as a ring cavity with a sensitivity of 1326 nm/RIU [25], and a circular split-ring resonator cavity with a sensitivity of 1114.3 nm/RIU [26]. Hajshahvaladi et al. [27] designed and investigated the highly sensitive nano ring resonators for RI sensing in the infra-red region. However, they showed that the nanoring sensor shows a high-sensitivity value of 2160 nm/RIU, it suffers from a weak FOM value of about 55.2 RIU⁻¹. A high-performance refractive index (RI) sensor was designed [19] based on plasmonic structures in the mid-infrared (NIR) and near-infrared (MIR) range. The sensor has a sensitivity of 5155 nm/RIU, but the resonance peak is wide, which may reduce the sensor resolution, as represented by the FOM. A highly sensitive RI sensor was constructed [28] based on a MIM waveguide with an irregular ring resonator. The sensor has a sensitivity and FOM of 2417 nm/RIU and 35 RIU⁻¹, respectively. From this profound, the designed plasmonic sensor must provide high-sensing performance for all parameters.

In this work, a highly sensitive MIM waveguide with nanoring resonators (MNR) is proposed for RI sensing based on coupling between them. The proposed structure is tested for RI sensing and shows three different coupling modes in the form of Fano resonance coupling. The appropriate parameters of the MNR such as nanoring resonator width are investigated and sensing performance parameters are reported. It is observed that the proposed sensor shows a sensitivity of 1700 nm/RIU, FOM of 4300.25 RIU⁻¹, and a quality factor of 4310. In addition, it acts as a multi-wavelength RI sensor, with sensing mode extremely sensitive to very small variations in the RI on the order of ±0.0004.

Structure

The Fano resonance phenomenon is a well-known optical effect that arises from the interference between two or more resonant modes in a photonic structure. When a resonant mode interacts with a continuum of states, it results in a characteristic asymmetric lineshape in the transmission or reflection spectrum. This phenomenon was first described by the Italian physicist Ugo Fano in 1961. In the context of a Fano resonance based on coupling between a nanoring resonator and a metal-insulator-metal (MIM) waveguide, the theoretical background can be understood as follows: The nanoring resonator and the MIM waveguide each have their own resonant

modes, which correspond to specific wavelengths of light that can be trapped and confined within these structures. When the resonant mode of the nanoring resonator couples with the continuum of modes in the MIM waveguide, their interactions lead to interference. This interference results in a Fano resonance profile in the transmission or reflection spectrum of the structure. The interference between the resonant mode and the continuum of states in the MIM waveguide creates an asymmetric lineshape in the spectrum. This lineshape is characterized by a sharp and narrow peak (resonance) superimposed on a broader background. The coupling between the nanoring resonator and the MIM waveguide can lead to regions of high electric field confinement within the structure. This enhanced field confinement is responsible for the sharp resonance peak observed in the spectrum. The Fano resonance is highly sensitive to changes in the surrounding environment, such as changes in refractive index. When the refractive index of the surrounding medium changes, it affects the resonant condition of the nanoring-MIM coupling, leading to shifts in the resonance wavelength. This sensitivity forms the basis for refractive index sensing applications.

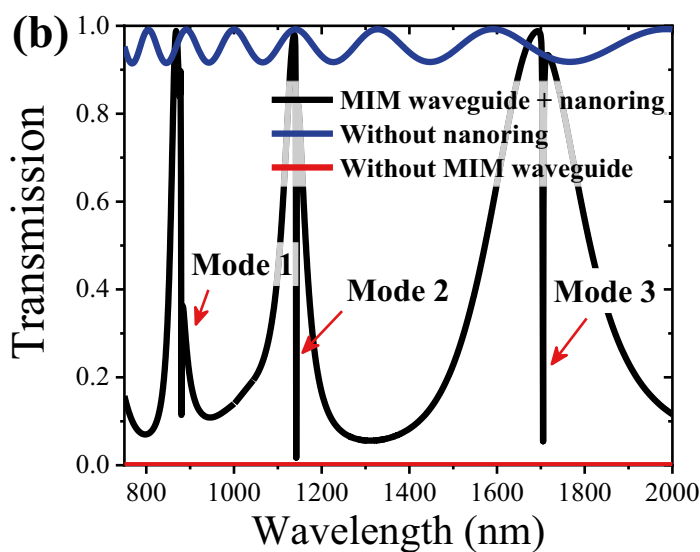
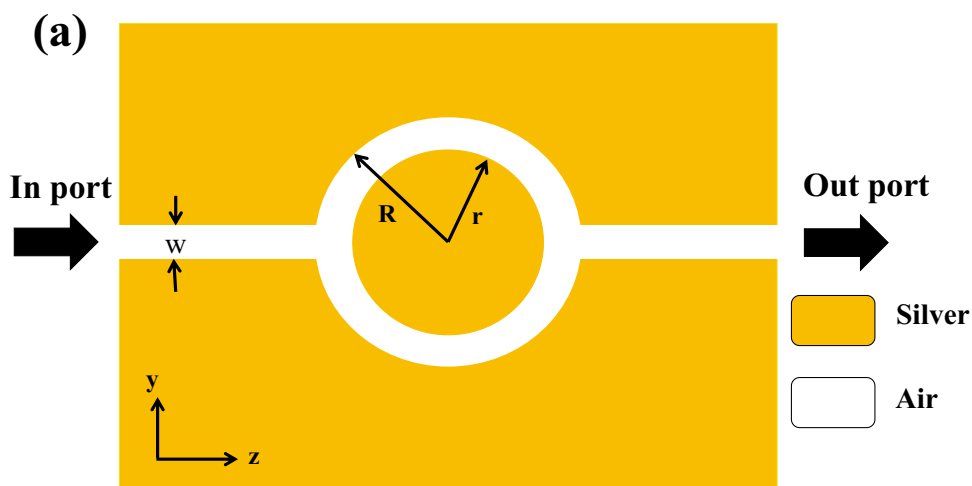
The proposed structure of the MNR RI sensor is illustrated in Fig. 1a. It can observe that the MIM with width $w = 50$ nm is coupled with a nanoring resonator with outer radius $R = 600$ nm and inner radius $r = 400$ nm. The width of the nanoring resonator (d) can be calculated as $d = R - r$. Through this design, the dielectric materials are air with relative permittivity $\epsilon = 1$, while the metal silver represented the widest-used plasmonic materials due to lower absorption compared with other metals [29]. The permittivity of silver $\epsilon_{(m)}$ is described by the well-known Drude Lorentz mode as follows [4]:

$$\epsilon_{(m)} = \epsilon_{\infty} - \frac{\omega_p^2}{\omega(\omega + i\gamma_p)} \tag{1}$$

where ϵ_{∞} is the dielectric permittivity of silver at infinity frequency, $\omega_p = 1.38 \times 10^{16}$ Hz is plasma frequency, $\gamma_p = 2.73 \times 10^{13}$ Hz is electron collision frequency, and ω represented the frequency of applied electromagnetic waves. By applying transverse magnetic (TM) mode through a designed MNR structure, the transmission spectrum can be evaluated. The simulation is performed using COMSOL simulation with very high meshed to more accurate results. In addition, the MNR surrounding are taken as a perfect match layer to concern the applied field in the proposed MNR sensor. The resonance wavelength of the proposed MNR sensor can be calculated from the following relation [30]:

$$\lambda_m = \frac{2Re(neff)L_{eff}}{m} \quad m = 1, 2, 3 \dots \dots \tag{2}$$

Fig. 1 a Schematic view of proposed MNR based on coupling between MIM waveguide and nanoring resonators, where $w = 50$ nm, $R = 600$ nm, and $r = 400$ nm. **b** The transmission spectra of the proposed MNR sensor in case of the presence and absence of the MIM waveguide and nanoring resonator, respectively



$$n_{\text{eff}} = \sqrt{\frac{\epsilon_{\text{air}} \times \epsilon_m}{\epsilon_{\text{air}} + \epsilon_m}} \tag{3}$$

where $\text{Re}(n_{\text{eff}})$ is the real part of the effective RI of the SPR, and L_{eff} is the effective resonance length of the nanoring resonator. The proposed structure's transmission spectra are shown in Fig. 1b in blue and red lines, respectively, for the cases of removing the nanoring resonator and MIM waveguide. Meanwhile, the black line in Fig. 1b shows the transmission spectrum of the proposed MNR. The proposed MNR sensor shows a zero transmission value when the MIM waveguide is removed, while it shows a set of constructive and destructive interference without a transmission dip when the nanoring resonator is removed. As a result, the three-transmission dip of the proposed MNR sensor can be explained as a coupling between the MIM waveguide and the nanoring resonator. Through this figure, three coupling modes are observed at resonance wavelengths of 880.24

nm, 1142.15 nm, and 1704.45 nm. The coupling between MIM and nanoring resonator through three different modes is displayed in the form of Fano resonance peaks with different symmetries. Hence, the proposed structure can act as a multi-wavelength RI sensor. The position of the resonance dip can be controlled by controlling the n_{eff} of the proposed MNR and sensor parameters represented in MIM width w and nanoring resonator width.

The three resonance modes show Fano peaks with full width at half maximum (FWHM) and transmission values of 0.265 nm, 92.6%, 0.337 nm, 97.98%, and 0.396 nm, 98.92% respectively. Recently, the high-performance sensor required a sharp edge and acceptable maximum transmission value. For the design of high-performance sensors, quality factor (Q) represented an essential that can be defined as the ratio between resonance wavelength λ_m and FWHM ($Q = \lambda_m/\text{FWHM}$) [22]. Thus, the three resonance modes provide a Q -factor of 3245.283 for mode 1, 3388.72 for

mode 2, and 4292.92 for mode 3. It can be observed that the third Fano resonance mode provides the highest value of the Q factor which will be good candidates for RI sensing. The zoom-in shape of three Fano resonance couplings is illustrated in Fig. 2 with the corresponding filed profile. The real (H_z) of the three coupling modes shows even symmetry along the horizontal and vertical axis. It can be obtained that the filed profile is fully coupled with high filed localization to the nanoring resonator via the narrow bus waveguide of the proposed MNR sensor. As a result, the coupling resonator will be sensitive to any change in the surrounding medium that will be promising for RI sensing.

Sensing Performance of the Proposed Sensor

The sensing ability of the proposed MNR can be investigated using several factors such as sensitivity, FOM, and Q factor. The sensing mechanism of such nanosensors is dependent on

shifts in resonance wavelength due to changes in n_{eff} caused by the change in insulator index. The sensitivity (S) can be defined as the shift in resonance wavelength $\Delta\lambda_m$ per change in RI Δn ($S = \Delta\lambda/\Delta n$) [31, 32]. Besides, FOM is another crucial that provide information about sensor resolutions and can be calculated from the relations [22]:

$$\text{FOM} = \frac{S}{\text{FWHM}} \tag{4}$$

Generally, Fano resonance modes are characteristic with sharp and high-sensitivity values that represent promising candidates for several applications such as RI sensing, switches, and modulators. Herein, the proposed MNR sensor generated three Fano resonance modes in the wavelength range from 800 to 2000 nm. However, the selected Fano dip should have high-sensing performances and gradual transitions. To demonstrate the most sensitive Fano resonance dip from three resonance modes, the RI of air is changed from 1 to 1.04 with constant step 0.01, and fix other parameters at $R = 600$ nm and

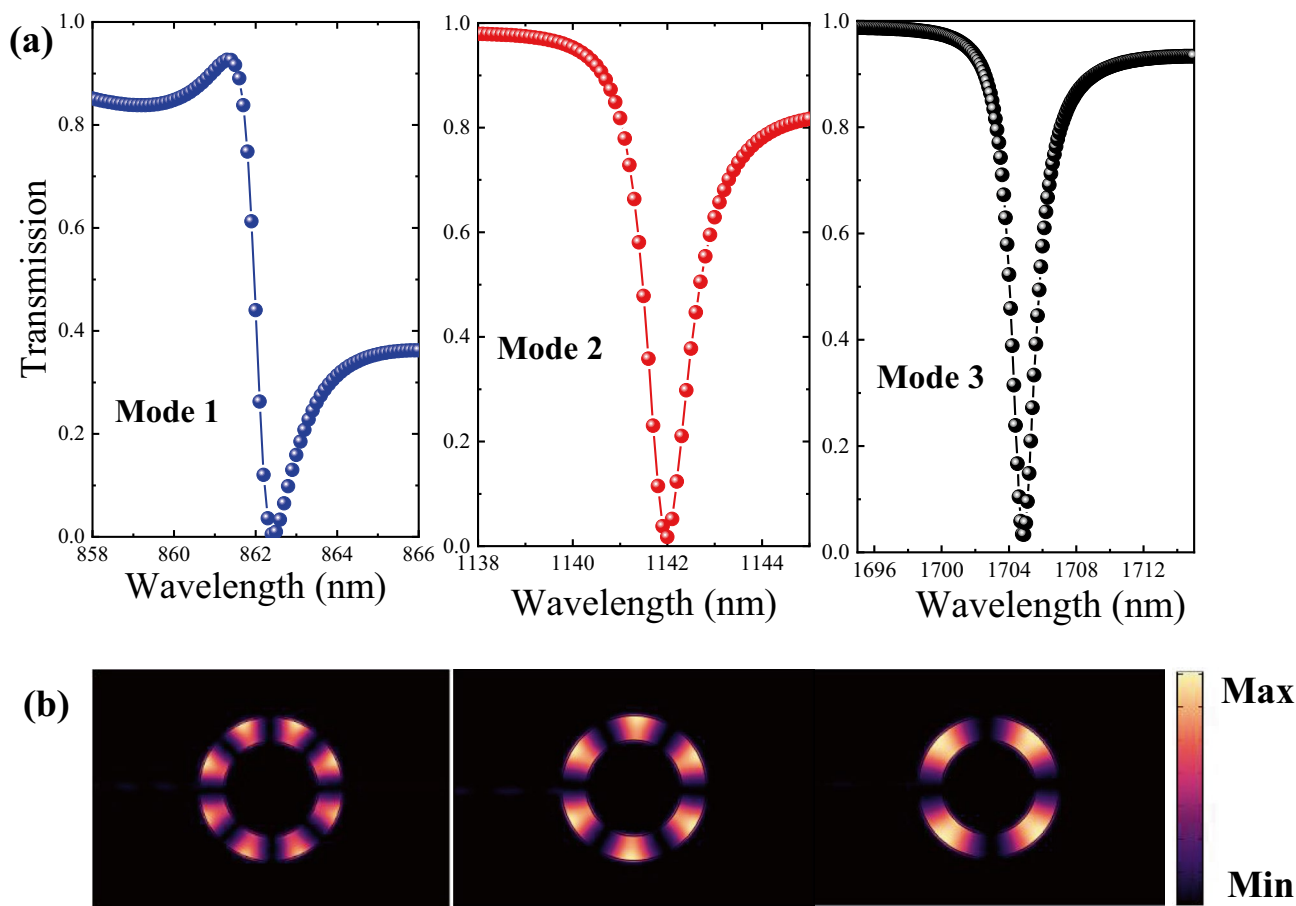


Fig. 2 **a** The zoom in shape for three Fano resonance peaks of three different coupling modes. **b** The corresponding magnetic field $|H_z|^2$ distributions of three modes

$r = 400$ nm. Consequently, the change in RI led to the shift of SPR wavelength and change in its propagation constant.

As illustrated in Fig. 3a–c, the plot of resonance wavelength λ vs. change in RI Δn with slope represented the value of sensitivity of each mode. It can be seen that mode 1 has a sensitivity value of 860 nm/RIU, mode 2 has 1140 nm/RIU, and mode 3 with a value of 1700 nm/RIU. From Fig. 3a–c, we can illustrate that the three-coupling mode has an approximately linear relationship with the RI of injected materials. As a result, the materials in turn can be recognized from the shift of resonance wavelength. Accordingly, the third resonance mode is the most acceptable mode for the proposed MNR for RI sensing. As illustrated in Fig. 4a, the transmission dip in spectra of the proposed MNR sensor shifts toward a higher wavelength as the RI of the insulator (n_{air}) increases. For $n_{air} = 1$,

the resonance wavelength appears at 1704.818 nm with full width at half maximum (FWHM) of 0.396 nm. The increase in the refractive index of air (n_{air}) leads to an increase in the effective refractive index (n_{eff}) of the MNR structure, according to Eq. (3). This increase in n_{eff} causes the transmission dip to shift to higher wavelengths and also reduces the FWHM value of the transmission dip. On the other hand, the design parameters of the nanoring, such as the outer radius (R) and inner radius (r), affect the value of the effective length (L_{eff}) of the sensor, and hence the sensing performance of the proposed MNR sensor [33]. It is known that the FOM parameter is used to indicate the selectivity and confirm the resolutions of the sensor [34–36]. Thus, the higher the FOM, the more selective the sensor is. Accordingly, the outer radius of the nanoring resonator is fixed at 600 nm and the inner radius r is swept

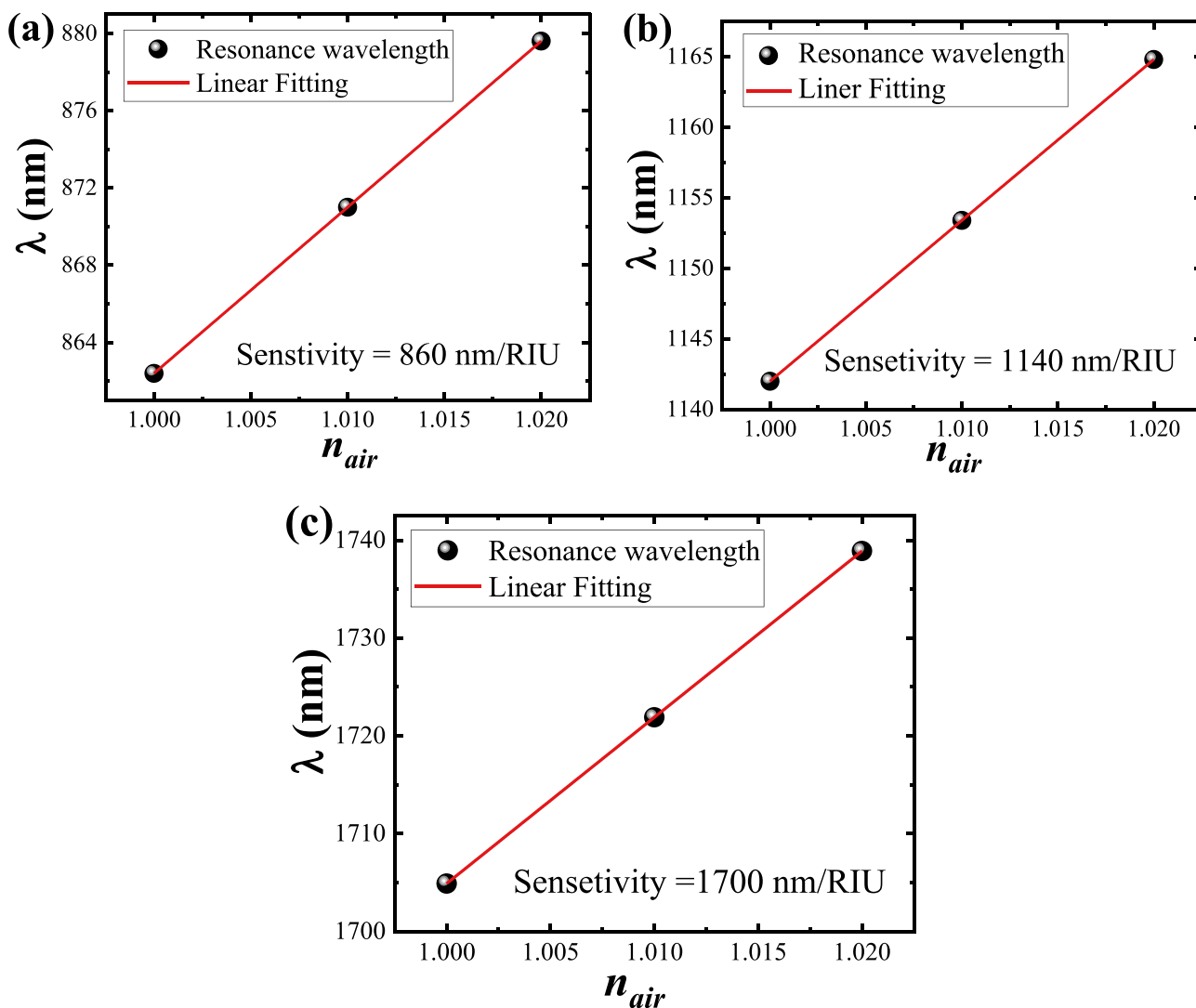


Fig. 3 The shift in resonance wavelength vs change in insulator RI, the black sphere represented the simulated result fitted by a solid red line and the slope represented the sensitivity value of **a** mode 1, **b** mode 2, and **c** mode 3

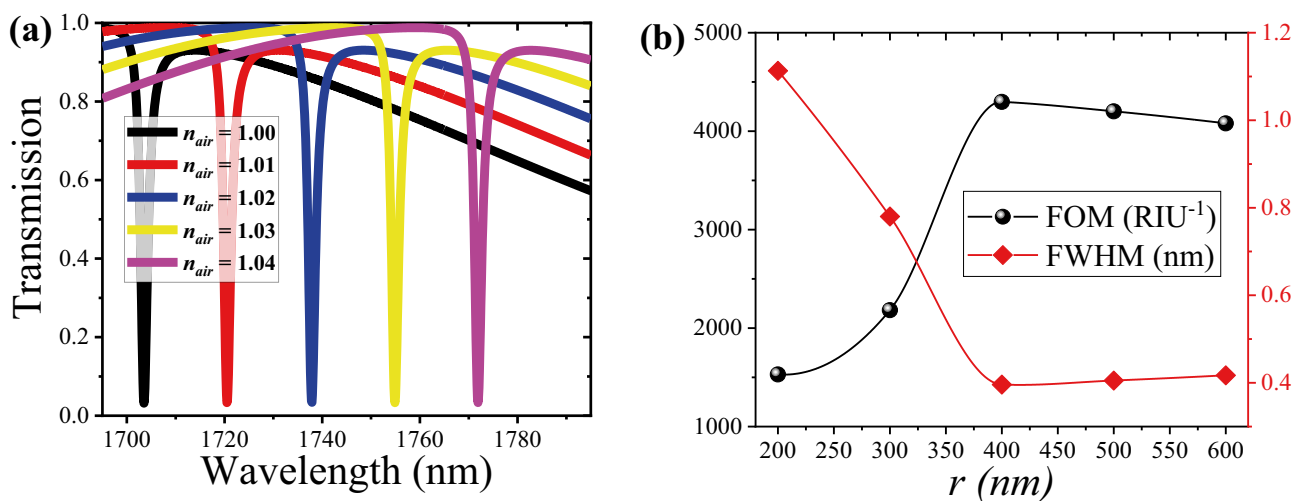


Fig. 4 **a** The transmission spectra of the proposed MNR sensor with different values n_{air} . **b** The FOM value as a function inner radius r of the nanoring resonator

to find the highest FOM value that is associated with high sensor resolution.

RAs displayed in Fig. 4b, the FOM and FWHM values are studied as a function of nanoring inner radius r . It can be observed that the FOM value increase with r until they reach the maximum at $r = 400$ nm (corresponding to nanoring width $d = R - r = 200$ nm), and then starts decreasing. On the other hand, the FWHM value shows the opposite trend. As the inner radius of the nanoring resonator (r) increases beyond 400 nm, the coupling strength between the MIM waveguide and the nanoring resonator decreases, resulting in a wider FWHM of the Fano peak. The coupling strength between two systems has a direct effect on the FWHM of the Fano peak, with stronger coupling leading to a narrower FWHM [23]. This is because the coupling strength determines the degree of overlap between the two systems' resonances. When the two resonances are strongly coupled, they overlap more completely, which results in a narrower FWHM. In the context of sensors, the Fano effect can be used to improve the sensor's resolution. A narrower FWHM means that the sensor is more sensitive to changes in the refractive index of the analyte. This is because the sensor can distinguish

between small changes in the analyte's refractive index more easily when the FWHM is narrower. As a result, this nanoring inner radius r would be an appropriate one for the proposed MNR for RI sensing that characteristic with a high FOM value. Indeed, almost every kind of active and passive integrated optic device based on the resonator is designed to work only with a selective frequency mode of propagation; the selectivity has been improved with respect to the presented designs. Another curial factor is the detection limit (DL) which can be calculated as follows: $DL = \lambda_m / QS$ [22, 31]. The value of DL means that the sensor can detect a very small change in RI that can be used in various applications with high efficiency. Further parameter to investigate the sensing performance of the proposed structure are detection accuracy (DA) and dynamic range (DR) that can be calculated by following relations $DA = 1 / FWHM$ and $DR = \lambda_c / \sqrt{FWHM}$ [37–39]. As FWHM gets smaller, DA and DR values get higher, and sensor performance gets better. The calculated values of sensing performance parameters are summarized in Table 1. Through this table, we can obtain that as the RI of the insulator materials (air in this case) increases, the Fano coupling are shift toward a higher wavelength and FWHM

Table 1 The sensing performance parameters of the proposed MNR

RI	λ_m (nm)	FWHM(nm)	Q	FOMFOM	DA	DR(nm)	DL(RIU ⁻¹)
1	1704.818	0.396	4.31×10^3	4300.25	2.53	2709.13	2.33×10^{-4}
1.01	1721.846	0.394	4.37×10^3	4323.18	2.54	2743.48	2.32×10^{-4}
1.02	1738.880	0.471	3.69×10^3	3613.20	2.12	2532.92	2.77×10^{-4}
1.03	1755.903	0.536	3.28×10^3	3177.05	1.87	2398.38	3.15×10^{-4}
1.04	1772.920	0.580	3.06×10^3	2925.945	1.718	2323.95	3.42×10^{-4}

is decreased. As a result, the Q factor and FOM decrease with increased analyte index.

Fabrication Technology

The proposed structural sensor's straightforward design makes it simple to manufacture in practice utilizing quick fabrication processes. The dimensions of the suggested sensor were chosen taking into account the 10 nm precision provided by the NIL (nanoimprint lithography) production technology. Compared to other lithographic fabrication techniques like EBL (electron beam lithography) and FIB (focused ion beam), this approach is characterized by low cost and high throughput [40]. The silicon wafer is first printed with silver patterns using the nanoimprint lithography (NIL) process [41, 42]. The remaining resin is then removed using oxygen plasma etching. Finally, an electron beam is used to evaporate a layer of silver onto the silicon wafer. This layer of silver covers the resin imprints, waveguides, nanoring, and other structures that have been formed in the lift-off process [43]. On the other hand, optical lithography with specially designed masks can be used to fabricate the structure contours, while focused ion beam milling can be used to realize the waveguide and nanoring at predetermined locations. This allows the proposed MNR structure to be fabricated in a single process without adding unnecessary complexity. The simplicity of the proposed sensor makes it suitable for fabrication with optical lithography techniques. On the other hand, FIB milling is utilized to materialize waveguides and nanoring at preset sites, while optical lithography with specifically created masks can also be employed to construct structural outlines. This allows for the simple fabrication of the proposed MNR structure in a single process without adding additional complexity. The proposed sensor is appropriate for manufacture using optical lithography techniques due to its simplicity [28, 44, 45].

To get a better understanding of the results, we compared the performance of the proposed MNR sensor with other plasmonic sensors in this section. The results are shown in Table 1. The comparison parameters include the FOM, sensitivity, Q factor, and DL of the resonance modes of the sensors. As shown in Table 1, the proposed MNR sensor has relatively suitable features in terms of all performance parameters. One of the main parameters is sensitivity. As mentioned before, although sensitivity can be a good characteristic for comparing sensors, it is not the only parameter. For example, Bahri et al. [19] have the highest sensitivity value in the comparison table, but its FOM value is low due to the resonance peak being wide. Although Rohimah et al. [46] proposed a sensor with high-sensitivity and ultra-high FOM value, it suffers

Table 2 Comparison of this work with the literature

Ref	Sensitivity (nm/RIU)	FOM (RIU ⁻¹)	Q	DL
[48]	937.5	143.44	140.122	-
[49]	750	20.58	21.84	-
[50]	1240.8	44.5	123.45	-
[47]	500	282.5	304.06	-
[19]	5155	-	-	-
[28]	2417	38	-	-
[46]	1636	33562	-	-
[51]	2800	333.3	-	-
[52]	3010	-	-	3.84×10^{-6}
[53]	7564	120	-	1.32×10^{-7}
[54]	2300	-	-	-
This work	1700	4300.25	4310	3.15×10^{-4}

from weak DL value. On the other hand, it is important to note that there is a trade-off between the design parameters of a sensor. For example, although Khani and Hayati [47] have a very high FOM among the reported works, it has eight resonance modes, which is not desirable. This is because the resonance modes of multi-mode sensors can interfere with each other when the resonance modes are shifted. Consequently, the high-performance sensor must achieve a high value of all sensing parameters. It is clear that previous studies have had weaknesses in one or more of the critical factors for building a sensor using different techniques. Sensor devices require high values of sensitivity, FOM, DL, and Q factor, which are key indicators for evaluating sensing ability and performance. We have developed an excellent and simple design platform for designing MIM RI sensors. This flexible platform can be used for any type of sensor by replacing the insulator materials with sensor materials. Therefore, our results may be helpful for the development of plasmonic optical sensors (Table 2).

Conclusion

In conclusion, we have proposed a Fano resonance sensor based on the coupling between a nanoring resonator and a MIM waveguide. The sensor exhibits a high sensitivity of 1700 nm/RIU, a FOM value of 4300.25 RIU⁻¹, and a quality factor of 4310. These results are comparable to the best-reported values for Fano resonance sensors. The proposed sensor is simple to fabricate and can be used for a wide range of RI-sensing applications. The high sensitivity of the sensor is due to the sharp and asymmetric Fano resonance. The FOM value is a measure of the robustness of the sensor to noise, and the Q factor is a measure of the bandwidth of the

sensor. The high values of these parameters indicate that the proposed sensor is a promising candidate for a variety of sensing applications. In future work, we plan to investigate the use of the proposed sensor for sensing other parameters, such as temperature and concentration. We also plan to improve the fabrication process of the sensor in order to achieve even higher sensitivities. We believe that the proposed sensor has the potential to be a valuable tool for a variety of sensing applications.

Acknowledgements The authors are thankful to the Deanship of Scientific Research at Najran University for funding this work under the Research Groups Funding program grant code (NU/RG/SERC/12/4).

Author Contribution The authors confirm their contribution to the paper as follows: study conception and design (Zain Elabdeen A. Mohamed). Software (Zain Elabdeen A. Mohamed). Draft manuscript preparation (Zain Elabdeen A. Mohamed). Editing the final version of the manuscript, correction of the language, response to reviews, and adding new figures to the revised version (Sofyan A. Taya, Abdulkarem H. M. Almagani, Ayman Taher Hindi). All authors reviewed the results and approved the final version of the manuscript.

Funding The authors are thankful to the Deanship of Scientific Research at Najran University for funding this work under the Research Groups Funding program grant code (NU/RG/SERC/12/4).

Data Availability The data that support the findings of this study are available from the corresponding author upon reasonable request.

Declarations

Ethical Approval Not applicable.

Competing Interests The authors declare no competing interests.

References

- Wang L, Zeng YP, Wang ZY, Xia XP, Liang QQ (2016) The energy separation effect based on the disk resonance multichannel MIM waveguide. *Mod Phys Lett B* 30(28):1650344
- Xie YY, He C, Li JC, Song TT, Zhang ZD, Mao Q-R (2016) Theoretical investigation of a plasmonic demultiplexer in MIM waveguide crossing with multiple side-coupled hexagonal resonators. *IEEE Photonics J* 8(5):1–12
- Livani AM, Kaatuzian H (2017) Modulation–frequency analysis of an electrically pumped plasmonic amplifier. *Plasmonics* 12:27–32
- Kaatuzian H, Taheri AN (2015) Applications of nano-scale plasmonic structures in design of stub filters—a step towards realization of plasmonic switches. *Photon Crystals* 93
- Zheng G, Chen Y, Xu L, Lai M, Liu Y (2013) Metal–insulator–metal waveguide-based band-pass filter with circular ring resonator containing Kerr nonlinear medium. *Opt Commun* 305:164–169
- Rastegar Pashaki E, Kaatuzian H, Mallah Livani A (2019) Hydrodynamic analysis and responsivity improvement of a metal/semiconductor/metal plasmonic detector. *Plasmonics* 14:1639–1648
- Lee TW, Kwon SH (2015) Dual-function metal–insulator–metal plasmonic optical filter. *IEEE Photonics J* 7(1):1–8
- Khani S, Danaie M, Rezaei P (2018) Realization of single-mode plasmonic bandpass filters using improved nanodisk resonators. *Opt Commun* 420:147–156
- Lai W, Wen K, Lin J, Guo Z, Hu Q, Fang Y (2018) Plasmonic filter and sensor based on a subwavelength end-coupled hexagonal resonator. *Appl Opt* 57(22):6369–6374
- Mao J, Zhai X, Wang L, Li H (2017) Numerical analysis of near-infrared plasmonic filter with high figure of merit based on Fano resonance. *Appl Phys Express* 10(8):082201
- Taheri AN, Kaatuzian H (2015) Numerical investigation of a nano-scale electro-plasmonic switch based on metal-insulator-metal stub filter. *Opt Quant Electron* 47:159–168
- Khani S, Danaie M, Rezaei P (2020) Compact and low-power all-optical surface plasmon switches with isolated pump and data waveguides and a rectangular cavity containing nano-silver strips. *Superlattices Microstruct* 141:106481
- Armaghani S, Khani S, Danaie M (2019) Design of all-optical graphene switches based on a Mach-Zehnder interferometer employing optical Kerr effect. *Superlattices Microstruct* 135:106244
- Danaie M, Shahzadi A (2019) Design of a high-resolution metal–insulator–metal plasmonic refractive index sensor based on a ring-shaped Si resonator. *Plasmonics* 14(6):1453–1465
- Lin Q et al (2016) A novel design of plasmon-induced absorption sensor. *Appl Phys Express* 9(6):062002
- Bensalah H, Hocini A, Bahri H (2022) Design and analysis of a mid-infrared ultra-high sensitive sensor based on metal-insulator-metal structure and its application for temperature and detection of glucose. *Prog Electromagn Res M* 112
- Brahmkhatri V, Pandit P, Rananaware P, D’Souza A, Kurkuri MD (2021) Recent progress in detection of chemical and biological toxins in water using plasmonic nanosensors. *Trends Environ Anal Chem* 30:e00117
- Ebadi SM, Örtegren J, Bayati MS, Ram SB (2020) A multi-purpose and highly-compact plasmonic filter based on metal-insulator-metal waveguides. *IEEE Photonics J* 12(3):1–9
- Bahri H et al (2022) A high-sensitivity biosensor based on a metal–insulator–metal diamond resonator and application for biochemical and environment detections. *Optik* 271:170083
- Salah HB, Bahri H, Hocini A, Zegaar I, Ingebrandt S, Pachauri V (2022) Design of a plasmonic sensor based on a nanosized structure for biochemical application. In: *Journal of Physics: Conference Series*, vol 2240, 1st edn. IOP Publishing, p 012021
- Abd-Elnaiem AM, Mohamed ZEA, Elshahat S, Almokhtar M, Norek M (2023) Recent progress in the fabrication of photonic crystals based on porous anodic materials. *Energies* 16(10):4032
- Elshahat S, Mohamed ZEA, Abd-Elnaiem AM, Ouyang Z, Almokhtar M (2022) One-dimensional topological photonic crystal for high-performance gas sensor. *Micro Nanostructures* 172:207447
- Khani S, Afsahi M (2023) Optical refractive index sensors based on plasmon-induced transparency phenomenon in a plasmonic waveguide coupled to stub and nano-disk resonators. *Plasmonics* 18(1):255–270
- Fang Y et al (2019) Multiple Fano resonances based on end-coupled semi-ring rectangular resonator. *IEEE Photonics J* 11(4):1–8
- Al-mahmod MJ, Hyder R, Islam MZ (2017) Numerical studies on a plasmonic temperature nanosensor based on a metal-insulator-metal ring resonator structure for optical integrated circuit applications. *Photonics Nanostructures-Fundam Appl* 25:52–57
- Wang M, Zhang M, Wang Y, Zhao R, Yan S (2019) Fano resonance in an asymmetric MIM waveguide structure and its application in a refractive index nanosensor. *Sensors* 19(4):791
- Hajshahvaladi L, Kaatuzian H, Danaie M, Karimi Y (2022) Design of a highly sensitive tunable plasmonic refractive index

- sensor based on a ring-shaped nano-resonator. *Opt Quant Electron* 54:1–17
28. Bensalah H, Hocini A, Bahri H, Khedrouche D, Ingebrandt S, Pachauri V (2022) A plasmonic refractive index sensor with high sensitivity and its application for temperature and detection of biomolecules. *J Opt* 1–12
 29. Ordal MA et al (1983) Optical properties of the metals al, co, cu, au, fe, pb, ni, pd, pt, ag, ti, and w in the infrared and far infrared. *Appl Opt* 22(7):1099–1119
 30. Hocini A, Ben Salah H, Khedrouche D, Melouki N (2020) A high-sensitive sensor and band-stop filter based on intersected double ring resonators in metal–insulator–metal structure. *Opt Quantum Electron* 52:1–10
 31. Elshahat S, Mohamed ZEA, Almokhtar M, Lu C (2022) High tunability and sensitivity of 1D topological photonic crystal heterostructure. *J Opt* 24(3):035004
 32. Hocini A, Ben Salah H, Temmar MNE (2021) Ultra-high-sensitive sensor based on a metal–insulator–metal waveguide coupled with cross cavity. *J Comput Electron* 20(3):1354–1362
 33. Luo X et al (2023) High-sensitivity long-range surface plasmon resonance sensing assisted by gold nanoring cavity arrays and nanocavity coupling. *Phys Chem Chem Phys* 25(13):9273–9281
 34. Le KQ, Ngo QM, Nguyen TK (2016) Nanostructured metal–insulator–metal metamaterials for refractive index biosensing applications: design, fabrication, and characterization. *IEEE J Sel Top Quantum Electron* 23(2):388–393
 35. Shrivastav AM, Cvelbar U, Abdulhalim I (2021) A comprehensive review on plasmonic-based biosensors used in viral diagnostics. *Commun Biol* 4(1):70
 36. Zafar R, Nawaz S, Singh G, d'Alessandro A, Salim M (2018) Plasmonics-based refractive index sensor for detection of hemoglobin concentration. *IEEE Sens J* 18(11):4372–4377
 37. Almawgani AH et al (2023) A photonic crystal based on porous silicon as a chemical sensor for the detection of methanol compound. *Indian J Phys* 1–10
 38. Taya SA, Shaheen SA (2018) Binary photonic crystal for refractometric applications (TE case). *Indian J Phys* 92(4):519–527
 39. Taya S (2018) Ternary photonic crystal with left-handed material layer for refractometric application. *Opto-Electron Rev* 26(3):236–241
 40. Jung WK, Byun KM (2011) Fabrication of nanoscale plasmonic structures and their applications to photonic devices and biosensors. *Biomed Eng Lett* 1:153–162
 41. Lee FY, Fung KH, Tang TL, Tam WY, Chan CT (2009) Fabrication of gold nano-particle arrays using two-dimensional templates from holographic lithography. *Curr Appl Phys* 9(4):820–825
 42. López-Muñoz GA et al (2017) A label-free nanostructured plasmonic biosensor based on Blu-ray discs with integrated microfluidics for sensitive biodetection. *Biosens Bioelectron* 96:260–267
 43. Kazanskiy N, Butt M, Khonina S (2020) Nanodots decorated MIM semi-ring resonator cavity for biochemical sensing applications. *Photonics Nanostructures-Fundam Appl* 42:100836
 44. Goyal AK, Dutta HS, Singh S, Kaur M, Husale S, Pal S (2016) Realization of large-scale photonic crystal cavity-based devices. *J Micro/Nanolithogr MEMS MOEMS* 15(3):031608–031608
 45. Dutta HS, Goyal AK, Singh S, Kaur M, Husale S, Pal S (2016) Fabrication of photonic crystal line defect waveguides by use of optical lithography and focused ion beam. In: *International Conference on Fibre Optics and Photonics*. Optica Publishing Group, p W4E.4
 46. Rohimah S et al (2022) Tunable multiple Fano resonances based on a plasmonic metal-insulator-metal structure for nano-sensing and plasma blood sensing applications. *Appl Opt* 61(6):1275–1283
 47. Khani S, Hayati M (2021) An ultra-high sensitive plasmonic refractive index sensor using an elliptical resonator and MIM waveguide. *Superlattices Microstruct* 156:106970
 48. Liu D et al (2019) Plasmon-induced transparency and refractive index sensing based on a trapezoid cavity coupled with a hexagonal resonator. *Plasmonics* 14:663–671
 49. Shahamat Y, Ghaffarinejad A, Vahedi M (2020) Plasmon induced transparency and refractive index sensing in two nanocavities and double nanodisk resonators. *Optik* 202:163618
 50. Alipour A, Mir A, Farmani A (2020) Ultra high-sensitivity and tunable dual-band perfect absorber as a plasmonic sensor. *Opt Laser Technol* 127:106201
 51. Chou Chao CT, Chou Chau YF, Chiang HP (2022) Breaking the symmetry of a metal–insulator–metal-based resonator for sensing applications. *Nanoscale Res Lett* 17(1):48
 52. Bahri H, Mouetsi S, Hocini A, Ben Salah H (2021) A high sensitive sensor using MIM waveguide coupled with a rectangular cavity with Fano resonance. *Opt Quantum Electron* 53(6):332
 53. Hassan MF, Sagor RH, Amin MR, Islam MR, Alam MS (2021) Point of care detection of blood electrolytes and glucose utilizing nano-dot enhanced plasmonic biosensor. *IEEE Sens J* 21(16):17749–17757
 54. Al Mahmud R, Sagor R, Khan M (2023) Surface plasmon refractive index biosensors: a review of optical fiber, multilayer 2D material and gratings, and MIM configurations. *Opt Laser Technol* 159:108939

Publisher's Note Springer Nature remains neutral with regard to jurisdictional claims in published maps and institutional affiliations.

Springer Nature or its licensor (e.g. a society or other partner) holds exclusive rights to this article under a publishing agreement with the author(s) or other rightsholder(s); author self-archiving of the accepted manuscript version of this article is solely governed by the terms of such publishing agreement and applicable law.